BJRS

BRAZILIAN JOURNAL
OF
RADIATION SCIENCES
08-03A (2020) 01-27

Analysis of the Heat Transfer Performance in a Brayton Cycle Recuperator

Araújo[a] E.F., Ribeiro[a] G.B., Guimarães[a] L.N.F.

[a] *Instituto de Estudos Avançados/ Divisão de Energia Nuclear, 12228-001, São José dos Campos, São Paulo, Brazil*
elvisaraujo15@gmail.com

ABSTRACT

Thermodynamic cycles are currently the most wanted means of converting nuclear power into available work due to the higher conversion efficiencies provided. Rankine cycles have been greatly applied for terrestrial reactors and nuclear submarines, while a lot of space projects have been using Brayton cycles for power conversion mainly due to mitigation in power-to-radiator area ratio. Regenerative Brayton cycles can present a considerable power conversion efficiency improvement when compared to the regular ones because of a reduction on the power demand from the hot heat exchanger of a cycle to achieve the same net output power. In this work, a cross-flow heat exchanger with He-Xe (40 g/mol) working fluid and Inconel 617 structural material used as the recuperator for the closed Brayton cycle of a nuclear reactor applicable for space systems is assessed in terms of heat transfer performance. The recuperator tubes are arranged in a staggered distribution around the exchanger axis. The matrix of tubes has a fixed count of 4 rows along the exchanger axis, while the number of tubes around the axis is variable, where the samples of 5, 7, 9, 12 and 16 are tested. The characteristic curves of heat transfer rate, effectiveness, convection coefficient and Colburn factor are built for each of the studied geometries in function of the Reynolds number. The obtained values for each of these parameters range between 1892.49 and 8493.21W (heat transfer rate), 0.165 and 0.325 (effectiveness), 60.3822 and 176.9682 W/m^{2}K (cold side convection coefficient), 30.3276 and 104.3263 W/m^{2}K (hot side convection coefficient), 0.0071 and 0.0109 (cold side Colburn factor), 0.0523 and 0.1370 (hot side Colburn factor).

Keywords: **Closed Brayton Cycle, Recuperator, Heat Transfer, Effectiveness, Convection.**

ISSN: 2319-0612
Accepted: 2020-11-12

1. INTRODUCTION

Nuclear reactors are currently seen as the best power source for space exploration vehicles due to several design advantages in comparison to their alternatives (solar, chemical and radioisotope), such as compact size, low mass, long operating lifetime, resistance to hostile environments and high reliability [1]. The power conversion of space nuclear-powered system designs along the last years has been mostly performed by thermoelectric, thermionic and thermodynamic systems. However, nowadays several research works have focused on thermal cycles due to their capacity of providing higher first law efficiencies [2]. This technology has a wide range of applications in multiple engineering fields, being used for power conversion in plants using various thermal energy inputs (solar, thermoelectric, nuclear, etc) and for propulsion and power supply in vehicles developed in the naval, auto, aeronautical and space industries.

Stirling, Rankine and Brayton cycles are widely used in several nuclear designs, where Stirling engines are primarily used in low power ranges (< 40 kW) [3,4]. In high power level regimes, Rankine cycles are mainly applied for power conversion in terrestrial and naval nuclear reactors, while Brayton cycles are more suitable for space nuclear power systems since they can provide a higher power-to-radiator area ratio [5], which is critical for mission success due to the need of minimum system sizes.

The majority of current power plants use regenerative heat transfer processes to allow higher cycle first law efficiencies [6-9]. The recuperator consists of a heat exchanger that makes thermal contact between the turbine and compressor outlets and increases the cycle efficiency by decreasing the heat demand from the hot source for a fixed output power. Therefore, improvements in the recuperator performance have a great impact on power conversion efficiency. In this context, the search for more compact heat exchangers has been occurring to fulfill industry needs for smaller and lighter equipment, mainly in areas such as biomedicine, fuel processing and aerospace [10]. The use of a compact and lightweight recuperator is critical for space applications, where low mass and volume are desired for the plant, allowing more science payload to be launched.

The trade-off between the heat transfer and pressure drop phenomena inside a heat exchanger is a classical approach which has been widely explored in several engineering applications [11-14]. In

the context of the growing demand for new performance assessments and improvements on dynamic thermal cycles, and considering that the space nuclear technology state-of-the-art always converged to compact plants with high power-to-mass ratio, the present work proposes a novel methodology for the evaluation of the thermal performance of a closed Brayton cycle (CBC) recuperator through CFD and heat transfer theory.

The recuperator under study is a cross-flow, shell-and-tube heat exchanger to be applied in a CBC applicable for a ≈ 200 kWe space nuclear reactor. It possesses multiple tubes whose quantity is not fixed by design. Besides, as it is part of a closed cycle with no working fluid bleed, inlet mass flow rates are necessarily the same for both streams. A parametric study is performed regarding number of tubes and inlet mass flow rate. The exchanger geometry is brought into the commercial CFD software Ansys Fluent (v. 18), where a physical model is built using data from the literature. The flow inside the recuperator is then solved with the Finite Volume Method (FVM) [15,16]. Several geometries are tested and multiple simulations are performed under different inlet mass flow rates, with further heat transfer analysis in the case post-processing.

2. NUMERICAL METHODOLOGY

This section describes the steps conducted throughout this work in order to investigate the thermal performance of the multiple CBC recuperator models simulated with different mass flow rate and number of tubes. The simulations demand the construction of a geometry suitable for CFD, followed by the usage of a mesh with satisfactory quality, the construction of the physical models from data on materials and boundary conditions, and the solution of the CFD cases using reliable methods validated through convergence monitoring. Furthermore, the heat transfer analysis performed in this work apply equations from heat transfer theory to information from the flow solution in the CFD post processing in order to evaluate the main parameters associated with the recuperator thermal performance.

2.1. Geometry and Mesh

The geometry used as a reference for the simulations draws inspiration from the CAD design of a modified NOELLE 60290 turbo starter, a turbomachine originally used as an Auxiliary Power Unit (APU) for the French aircraft *Mirage*. The former geometry and the actual design for CFD are respectively shown in Figures 1 (a) and (b). The prior CAD design shown in the left adapts the APU into the arrangement of a CBC. The recuperator, shown in green, is a shell-and-tube heat exchanger, where the tubes are oriented in a 30º deviation from the radius, which increases the heat transfer area *A* an orients the tube flow outlet in a lower angular deviation from the heat source inlet, shown in dark blue in Figure 1 (a), and consequently reduces head losses induced by flow direction change.

Figure 1: Design of modified NOELLE 60290 for CBC (a). Geometry used for CFD (b).

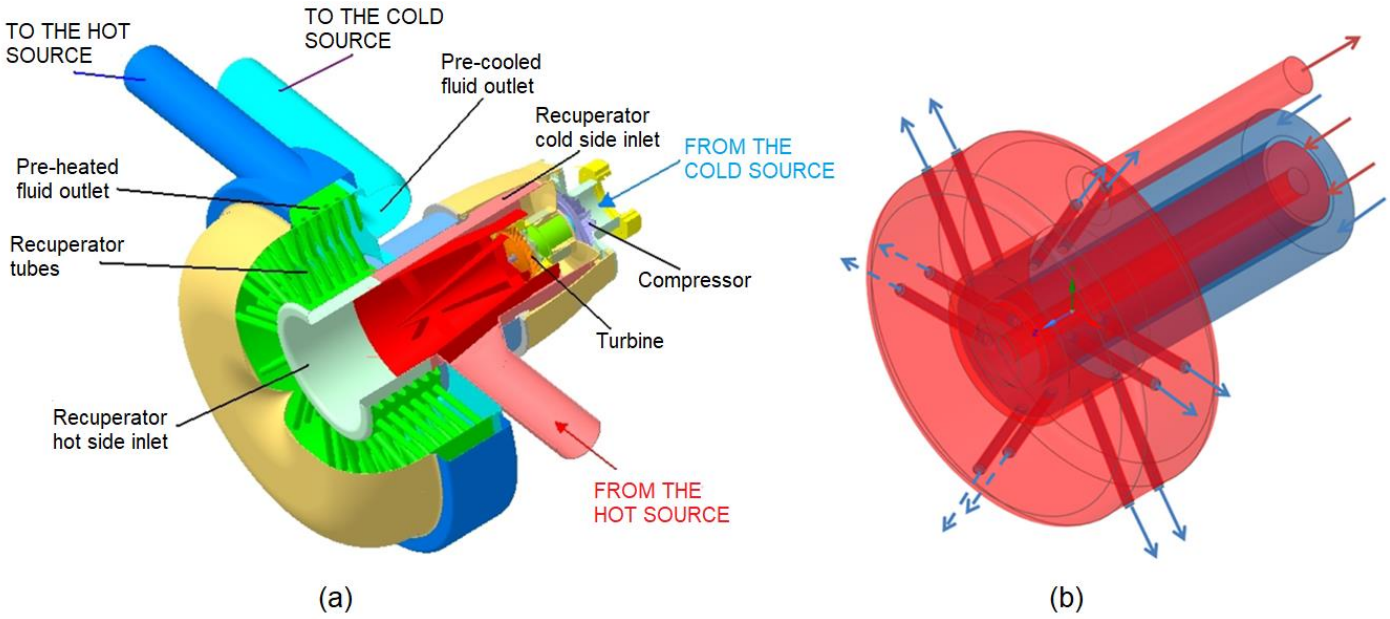

Source: adapted from [17].

This work is focused in the recuperator heat transfer mechanism, thus the CFD geometries are solely the cold and hot streams and the tubes through which heat is conducted. The diameter of the tubes in the recuperator remains constant through the tests because reducing its size would threat

the feasibility of its manufacturing, and higher diameters could compromise the quality of mesh elements in between the tubes, mainly close to the center channel. In this study, there is a constraint of fixed recuperator volume, which is motivated by the fact that this component is usually one the major volumes in space nuclear power plants, being only overwhelmed by the radiator panels [18], and volume is desired to be minimal in space applications. Therefore, geometrical parameters that affect the recuperator overall volume such as tube pitch, tube length, diameter of the heat exchanger shell size and number of tube rows distributed axially are kept fixed, while the number of ducts around the axis varies. The geometries with 4 rows of 5, 7, 9, 12 and 16 tubes are studied. In this document, the variable n_t is used to index a given geometry by its total number of tubes. Figure 1 (b) includes arrows to indicate the ends of each stream. The cold fluid flows in an external trajectory and then splits into the tubes (exchanger tube side), while the hot stream flows in an internal trajectory, fills the exchanger shell side and then exits the domain through the outlet duct. The geometry is oriented in the z direction, with $z = 0$ at the inlet of the first tube row.

Figure 2: Dimensions of the geometry used for CFD simulations. (a) Right view, with cold and hot domain ends respectively marked by blue and red arrows. (b) Front view.

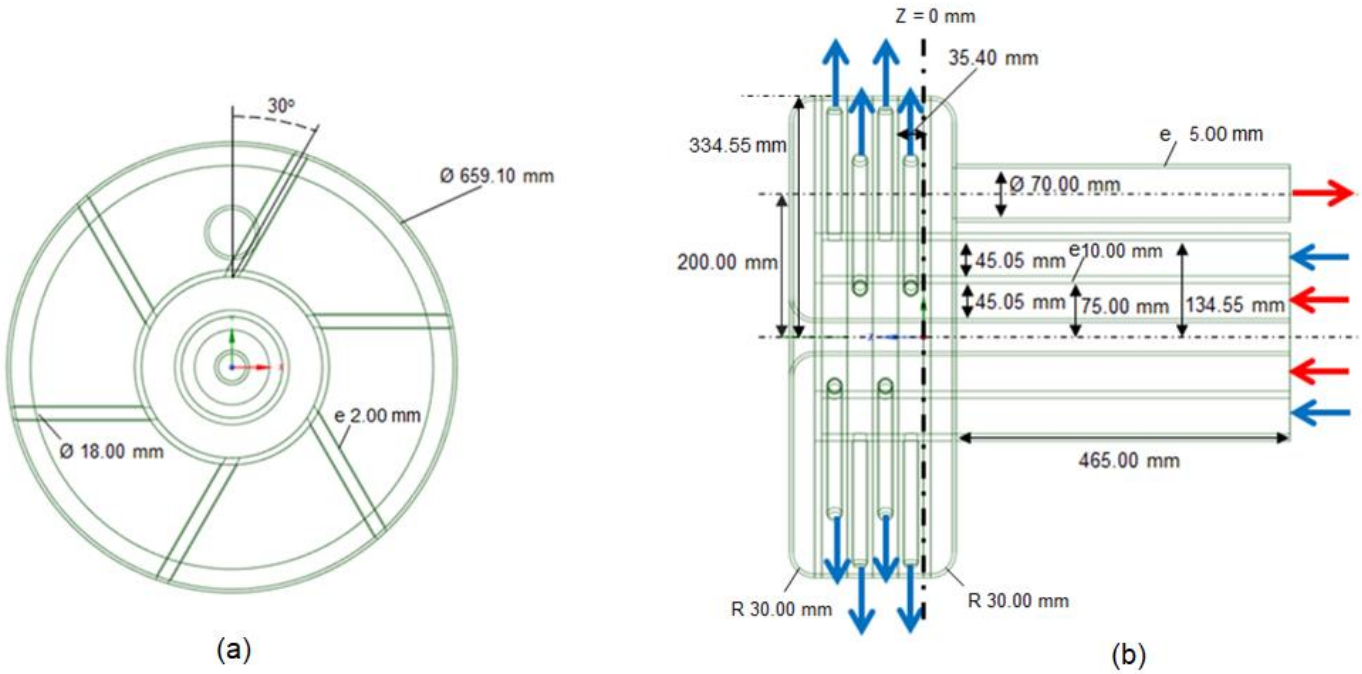

Source: from author.

The tubes are distributed in a staggered configuration along the axis, which avoids flow stagnation between consecutive tubes and reduces the number of small regions between these tubes, enhancing the feasibility for mesh generation. The main dimensions of the geometry under study are shown in Figure 2. The 0.465 m length applied between the inlets and the heat transfer region prevents a uniform flow profile in the entrance of the heat exchanger. The hot outlet is extruded in the same distance to prevent backflow in the intermediate flow solutions during CFD calculation.

The meshing procedure was focused in providing a grid that could properly catch the conduction and convection mechanisms within the interfaces between the two streams and also provide good quality elements to support the FVM calculations. Both domains are segmented into inlet, center and outlet sections for the meshing process. This division supports the confection of computationally efficient meshes because of the geometrical particularities of each region, which demands distinct approaches for mesh generation. It can be seen in Figure 3. The heat exchanger (HX) core is formed by the cold outlet section (tube side) and the hot center section (shell side).

Figure 3: Cold (a) a hot (b) domain division for mesh generation.

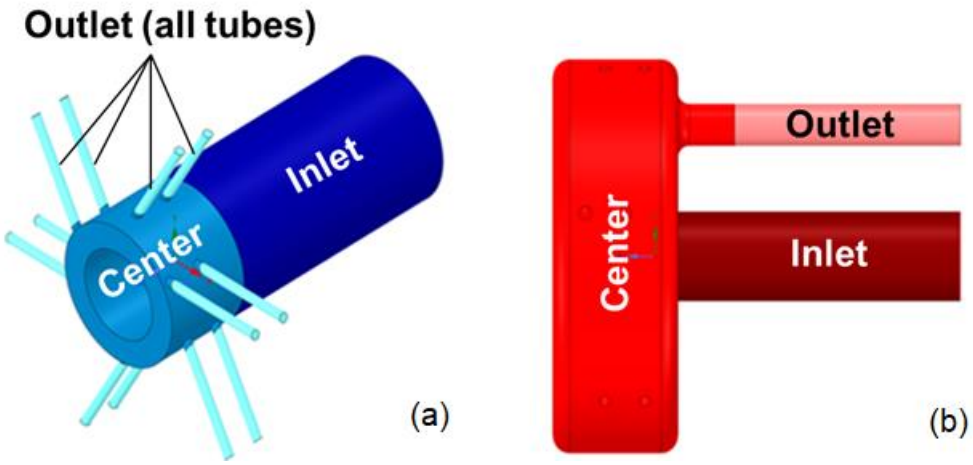

Source: from author.

Hexahedral elements are applied to regions with constant cross section, in this case, the inlets and outlets of both streams. The element size referred as the variable *l* (in millimeters) is used in the

cold outlet, while a $2l$ + 2 mm sizing is used in the inlets and the hot outlet. The remaining HX regions are meshed with tetrahedral elements afterwards in a shared topology scheme (matching grids between common faces of neighboring bodies) and with a $2l$ + 2 mm face sizing in the internal and external faces of the hot center due to the higher temperature gradients expected in this region. Furthermore, three layers of prismatic elements are applied close to the borders of the fluid entities to improve the boundary layer catch precision. Figure 4 shows an example of the recuperator grid with l = 4 mm.

Figure 4: Recuperator grid topology with l = 4 mm.

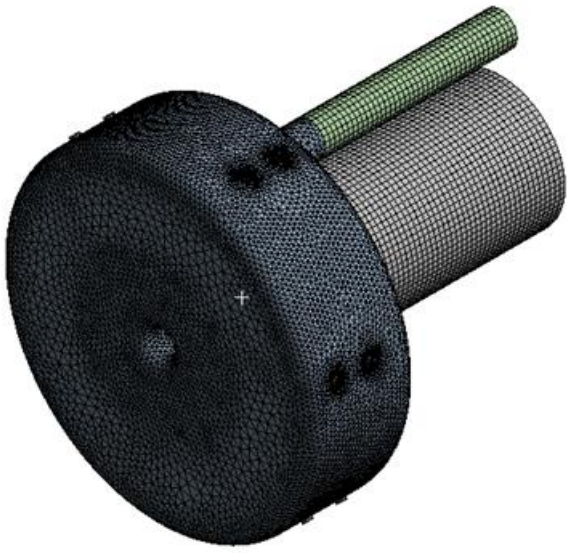

Source: from author.

2.2. Mathematical Model and Solution

The construction of the physical model to be considered by Ansys Fluent is inspired by the documentation on design decisions of a prior NASA project applying a CBC as power conversion technology [19]. The materials selected for the fluid and solid bodies in this work are respectively a 40 g/mol He-Xe mixture and the metallic alloy Inconel 617. The He-Xe mixture has good thermophysical properties, such as a high heat capacity, which enhances the heat transfer rate, and

the reasonably high fluid molecular weight reduces the needed number of turbomachinery stages, whereas Inconel 617 is suitable for operation in high temperatures.

The model inlet temperatures are respectively 538 K and 943 K for the cold and hot inlets. Velocity and temperature at the entrances of each stream are considered uniform over the cross-section, and atmospheric pressure (101325 Pa) is assumed on the outlets. Heat transfer is assumed to solely occur through the tubes walls since all other model surfaces are set as adiabatic. Inlet mass flow rates are the same for both HX sides due to its applicability in a CBC with no recuperator bleed fluid.

The mechanical feasibility of using Inconel 617 in this application is supported by several Alloy 617 creep and creep-rupture tests in 800-1000 ºC performed by the Idaho National Laboratory (INL) and Korea Atomic Energy Research Institute (KAERI) and compiled by Wright *et al.* [20]. The Larson Miller analysis for 10-15% Co Inconel 617 at 1000 ºC revealed a creep-rupture time of nearly 20.9 years under 7 MPa, thus proving the solid material creep resistance for the temperatures in this case-of-study, as the thresholds for pressure and temperature are significantly higher than the maximum values previewed by Ashcroft and Eshelman [19] (1150 K and 2 MPa), and the system under study is intended to last for 15 years.

The flow inside the recuperator is subsonic ($M < 0.3$), thus the incompressible approach can be used without a considerable accuracy loss. Fluid density is therefore computed through the state equation for ideal incompressible gases

$$\rho = p_{op}/RT \tag{1}$$

where p_{op} is the operating pressure. This equation is valid for He-Xe mixtures with less than 60 g/mol molecular weight [20]. Material thermophysical properties for Inconel 617 [21] and He-Xe 40 g/mol [22] inserted into the recuperator physical model are displayed in Table 1. The properties of the fluid entity vary with temperature, thus a linear interpolation is assumed. Flow is considered in the steady-state.

Table 1: Material Properties.

Property	**Inconel 617**	**He-Xe**
k [W/mK]	18.825	0.08409 (400 K) - 0.18340 (1200 K)
c_p [J/kgK]	500	535.7 (400 K) - 519.7 (1200 K)
ρ [kg/m^3]	8360	State Equation
μ [10^{-6} Pa·s]	-	32.857 (400 K) - 74.286 (1200 K)

Turbulence is modeled with the k - ϵ model thus the governing equations over the HX internal flow are the balances of mass (continuity), linear momentum, energy, turbulent kinetic energy and turbulent dissipation rate, in a total of 7 governing equations, as the momentum has to be conserved in x, y and z. The differential governing equation for continuity is expressed by

$$\nabla \cdot (\rho \vec{u}) = 0 \tag{2}$$

where ρ stands for the fluid density, and $\vec{u}$ is the velocity vector. The left-hand side denotes the infinitesimal net mass flux. The differential equation for linear momentum conservation is

$$\nabla \cdot (\rho \vec{u}\vec{u}) = -\nabla p + \nabla \cdot \bar{\bar{\tau}} \tag{3}$$

Here, the body forces are neglected due to the absence of gravity. The left-hand side is the net linear momentum flux, and the terms in the right-hand side respond for the sum of forces on a fluid differential element. In this equation, the term $\bar{\bar{\tau}}$ is the viscous stress tensor for a Newtonian fluid, which can be expressed in a Cartesian system by equation 3.

$$\bar{\bar{\tau}}_{ij} = \mu \left(\frac{\partial u_i}{\partial x_j} + \frac{\partial u_j}{\partial x_i} \right) - \frac{2\mu}{3} (\nabla \cdot \vec{u}) \tag{4}$$

Finally, the differential equation representing the conservation of energy within a fluid element is

$$\nabla \cdot (\rho \vec{u} c_p T) = -\nabla \cdot (k \nabla T) \quad (5)$$

Here, the rate of change of energy within a fluid elementary volume equals the sum of the rate of heat added to and the rate of work done on it. Neglecting the compressibility effects, the left-hand side responds for the net enthalpy flux, whereas the term in the right-hand side is the net rate of heat transfer through conduction. The variable *T* denotes the temperature and the term *k* stands for the thermal conductivity.

In this work, the Least Squares Cell-Based (LSCB) method is used to compute the gradient of a given value, while the First Order Upwind (FOU) method is the chosen spatial discretization scheme to interpolate property values at cell faces from cell center values. The accuracy of this method was found to be similar to the results obtained using second-order schemes, with the benefit of demanding less simulation time.

The pressure-based solver is preferred over the density-based one due to the incompressible flow. The determination of the velocity field along the flow domain is performed through a coupled solution, where the discretized mass and momentum equations are solved simultaneously from a prior guessed or iterated solution, resulting in the pressure and velocity fields, followed by the solution of the energy, turbulent kinetic energy, and dissipation rate equations.

The linear system produced by the discretization process is solved iteratively. Convergence is assumed as achieved when residues fall below their tolerances, system physical properties stabilize and total mass and energy imbalances are insignificant. The solution modification between two iterations is performed by an update with under-relaxation factors. In this work, residue tolerances are 10^{-6} for energy and 10^{-3} for continuity, momentum, turbulent kinetic energy and dissipation rate, whereas under-relaxation factors are 0.8 for turbulence kinetic energy and dissipation rate and 1 for density, body forces, turbulent viscosity and energy. Inlet pressures and outlet temperatures are used as solution monitors.

2.3. Heat Transfer Analysis

This section explains the procedure for determination of the thermal parameters used in this work to characterize heat transfer between the two fluids inside the CBC recuperator. Like explained earlier, the streams are separated by a heat transfer wall, where the main mechanism of heat transmission is convection from the hot fluid to the wall hot surface, conduction between the two wall faces, and then convection from the wall cold surface to the cold fluid, which characterizes an arrangement of three thermal resistances in series.

For the sake of simplicity, a single-pass, counter flow heat exchanger is considered. Several other assumptions are made for performing this heat transfer analysis in addition to those made during the mathematical model step, inspired by Shah and Sekulic [23]: temperature of each fluid is uniform over every cross section, wall thermal resistance is distributed uniformly in the entire exchanger, longitudinal heat conduction in the fluids and in the wall are negligible, the overall heat transfer coefficient and the specific heat are constant throughout the exchanger (the arithmetic mean between inlet and outlet values is assumed), and the heat transfer surface area is distributed uniformly on each fluid side. The exchanger flow simulation results are used as inputs for the heat transfer assessment through equations from theory explained below.

The heat transfer rate Q is computed from the temperature gradient suffered by the cold fluid, being expressed mathematically by equation 5. From the exchanger energy balance, the heat transfer rate is the same for both sides.

$$Q = \dot{m} c_p \Delta T \tag{6}$$

The overall thermal conductance UA is related to the heat transfer rate and the temperature gradient from the rate equation

$$Q = UA\Delta T \tag{7}$$

where ΔT_m is the mean temperature difference between the streams. From a thermal resistance standpoint, UA measures the heat flow per degree of temperature gradient, being an indicator of the how intense does a given exchanger arrangement allows heat to flow under a certain inlet temperature difference. In this work, the log-mean temperature difference expressed by equation 7

is used for being valid for counterflow exchangers [23], where the subscripts identify HX side and end referred by each temperature.

$$\Delta T_m = \frac{(T_{hi} - T_{co}) - (T_{ho} - T_{ci})}{\ln \frac{T_{hi} - T_{co}}{T_{ho} - T_{ci}}} \tag{8}$$

The effectiveness ε is defined as the ratio between the actual heat transfer rate and the one associated to an ideal exchanger with infinite surface area operating with the same fluid flow rates and inlet temperatures as the actual HX [22]. Since this work considers equal capacity rates for both fluid streams, the expression for effectiveness yields

$$\varepsilon = \frac{T_{co} - T_{ci}}{T_{hi} - T_{ci}} = \frac{T_{hi} - T_{ho}}{T_{hi} - T_{ci}} \tag{9}$$

The convection heat transfer coefficient h associated to a solid-fluid interface is equal to the ratio between the actual heat transfer occurring through convection Q and the temperature difference between the value at the wall T_w and the flow bulk value T_m [22]:

$$Q = h(T_w - T_m) \tag{10}$$

The peripheral wall temperature formula described by equation 10 is used to evaluate the wall temperature, where P is the duct perimeter and s is the spatial coordinate at a point on the duct wall (of finite thickness) along the inside perimeter. In this work, this parameter is calculated with the Ansys Fluent CFD post processing tool.

$$T_{w,m} = \frac{1}{p} \int_p T_w ds \tag{11}$$

The Colburn factor *j* is a dimensionless representation of the heat transfer coefficient and is defined as

$$j = StPr^{2/3} = \frac{Gc_p}{h}Pr^{2/3} \tag{12}$$

Where *St* is the Stanton number, which represents the ratio of convected heat transfer (per unit duct surface area) to the enthalpy rate change of the fluid reaching the wall temperature (per unit flow of cross-sectional area), $G = \rho u$ is the mass velocity and *Pr* is the Prandt number, which is defined by the ratio between momentum diffusivity and thermal diffusivity and is solely a fluid property modulus, being inserted into this formula to account for material influence in heat transfer [22]. The Prandt number of the working fluid under study is 0.71 [20].

The thermal assessment of the recuperator is performed through the evaluation of *Q*, *UA*, ε, *h* and *j* (the last two for both HX sides) through respectively equations 5, 6, 9 and 11. The variables that appear in these equations are extracted for each CFD case in Ansys Fluent after CFD case solution with the post processing tool available for this software. The bulk fluid temperature T_m used in eq. 9 for the convection heat transfer coefficient is assumed as the arithmetic mean between the mass-weighted average inlet and outlet temperatures.

3. RESULTS AND DISCUSSION

3.1. Mesh Independence Check

It is known that the computational mesh has to be in conformity with the physical phenomena, with a higher refinement in regions of greater property variation, in order to properly capture domain geometric details. Besides, it has to be free of bad quality elements that can lead to convergence problems and numerical errors. On the other hand, excessive refinement can produce unnecessary computational cost without a significant accuracy enhancement. Therefore, the sensitivity analysis related to mesh refinement has to be assessed so the mesh which best combines satisfactory results and low computational cost can be found. The chosen mesh should produce approximately

the same results of the grid with the largest number of elements. Using the mesh generation algorithm previously described, multiple CFD cases were solved using distinct grids with fixed geometry (12 tubes) and boundary conditions ($\dot{m}$ = 0.1 kg/s). In the post-processing step, the temperatures of 26 evenly spaced points along the center line of the middle tube located in the recuperator first row are evaluated for each solution. All mesh sizes are indexed by the characteristic length *l*. The distribution of the fluid temperature along the tube length for different mesh sizes is displayed in Figure 5.

Figure 5: Temperature profiles obtained for multiple meshes with fixed geometry (12 tubes) and inlet mass flow rate (0.1 kg/s).

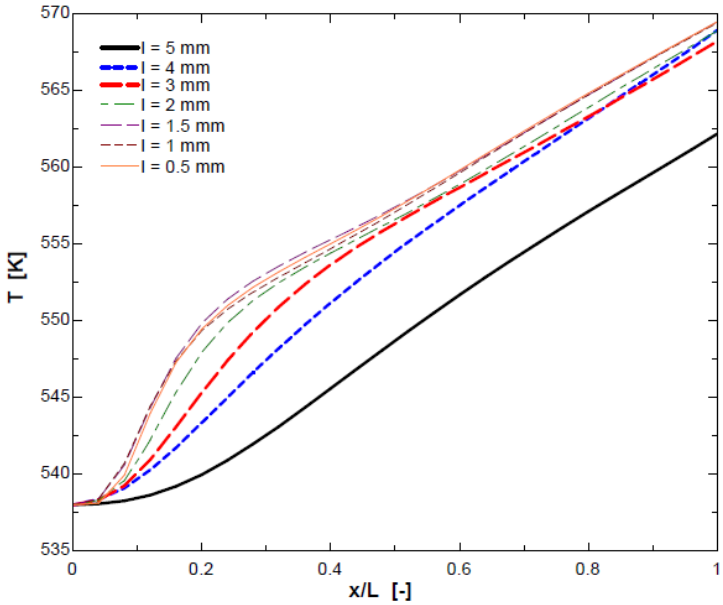

Source : from author.

The recuperator configuration with 12 tubes is the chosen geometry used for the grid refinement sensitivity study due to its simplicity, reducing the computational cost for the evaluation of *l* associated with the optimized grid which defines the mesh sizes in all other configurations. However, the geometry with 12 tubes is not assessed in the second law analysis because of the low-temperature difference obtained from flow solution. For the mesh independency check procedure, variable *e* is set as the analysis parameter as follows

$$e = \max \frac{T_{g1}^{i} - T_{g2}^{i}}{T_{g2}^{25} - T_{g2}^{0}} \tag{13}$$

where e is defined as the maximum relative error between the mesh results of two consecutive grids in the refinement scale. The subscripts *g1* and *g2* refer to the fine and the coarse grids, respectively, and the superscript *i* represents the point where the temperatures are compared.

The maximum relative error between the chosen mesh and more refined ones must be lower than a given tolerance. In this work, the criterion for mesh selection is the coarser grid in a group of three consecutive meshes associated with two errors e_1 and e_2 such that e_1, $e_2 < 0.05$. Table 2 shows the error values obtained and the number of elements for each simulated grid. Simulation time and memory usage increases substantially with the grid element count. Based on the criterion described previously, meshes indexed by l = 1.5 mm are applied for all other recuperator configurations.

Table 2: Maximum relative errors and number of elements.

***l* [mm]**	***e* [-]**	**Number of elements [-]**
5	0.222	984510
4	0.089	1254307
3	0.104	1747957
2	0.126	3521590
1.5	0.042	6317637
1	0.047	15821218
0.5	-	80746464

3.2. Thermal Parameters

This section presents the results obtained from the measurement of heat transfer metrics associated with the HX under study. Like explained before, it is done through the use of several equations from heat transfer theory (equations 5 to 11) to data on the recuperator temperature fields

obtained from CFD simulations. The results are plotted against the arithmetic mean of inlet Reynolds numbers of the two HX streams.

Figure 6 shows the heat transfer rate *Q* curves obtained for the studied geometries, each one fitted into its Reynolds number range-of-test. It can be seen that it increases with flow velocity, which is expected from a physical standpoint since more mass is exchanging heat per under a fixed inlet temperature difference, the heat transfer driving force. The increase in number of tubes is responsible for heat transfer augmentation because of the raise in heat transfer area.

Figure 6: Profiles for heat transfer rate *Q* against inlet Reynolds number *Re* obtained for the 5 recuperator geometries.

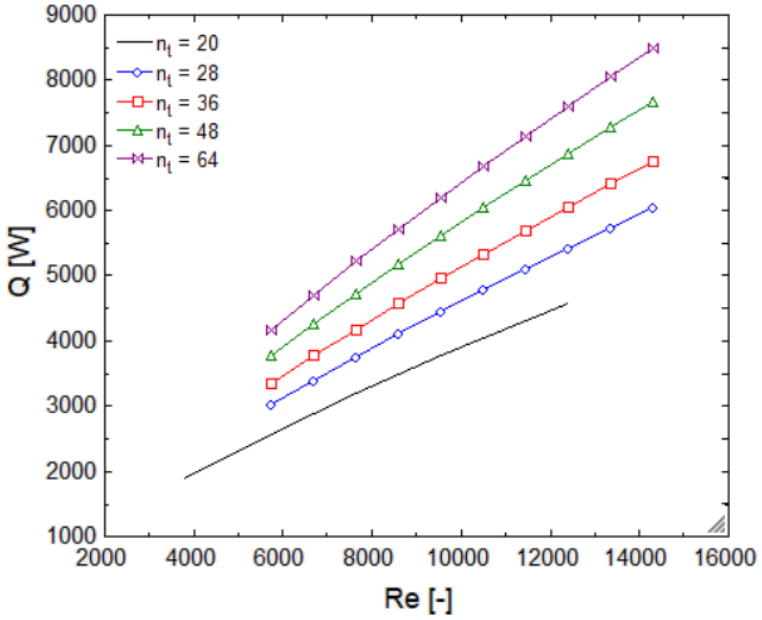

Source: from author.

Figure 7 describes the influence of HX geometry and inlet Reynolds number on the HX effectiveness ε. It can be observed that, oppositely to the heat transfer *Q*, this parameter has a decreasing relationship with flow velocity. This effect is physically explained by the fixed heat transfer driving force (inlet temperature difference) and the raising heat capacity rate as the mass flow rate increases, which reduces the fluid temperature gradient, even though the heat flux increases with fluid velocity because of its positive impact on the convection heat transfer coefficient. Like

expected, the effectiveness rises with number of tubes due to heat transfer area increase, which increases the temperature gradient suffered by the two HX fluids.

The effectiveness values obtained are relatively low (the maximum value is approximately 0.4) when compared to values predicted for space nuclear designs such as the ones described by [18] and [7], where ε is supposed to reach 0.92 and 0.95 respectively, which suggests the need for a HX geometry redesign with a higher heat transfer area, for example, with the inclusion of fins alongside the recuperator tubes.

Figure 8 plots the overall thermal conductance *UA* against inlet Reynolds number *Re* for the studied recuperator geometries. Physically, an exchanger with a higher *UA* imposes a lower resistance to heat flow with the same inlet temperature difference, thus there is a thermal circuit analogy where *1/UA* plays the role of the equivalent resistance [24].

In the tested inlet mass flow rate range, *UA* increases nearly in a linear fashion with flow velocity, which is evidenced by the heat transfer rate rise and effectiveness loss caused by this effect (from equation 6, $UA = Q/\Delta T$). Other explanation for *UA* increase with the Reynolds number is the well-known positive dependence between the convection heat transfer coefficient and the flow bulk velocity. Furthermore, it can be observed that the overall thermal conductance rises with number of tubes because of heat transfer area enhancement with a consequent thermal resistance decrease.

Figure 7 : Profiles for effectiveness ε against inlet Reynolds number *Re* obtained for the 5 recuperator geometries.

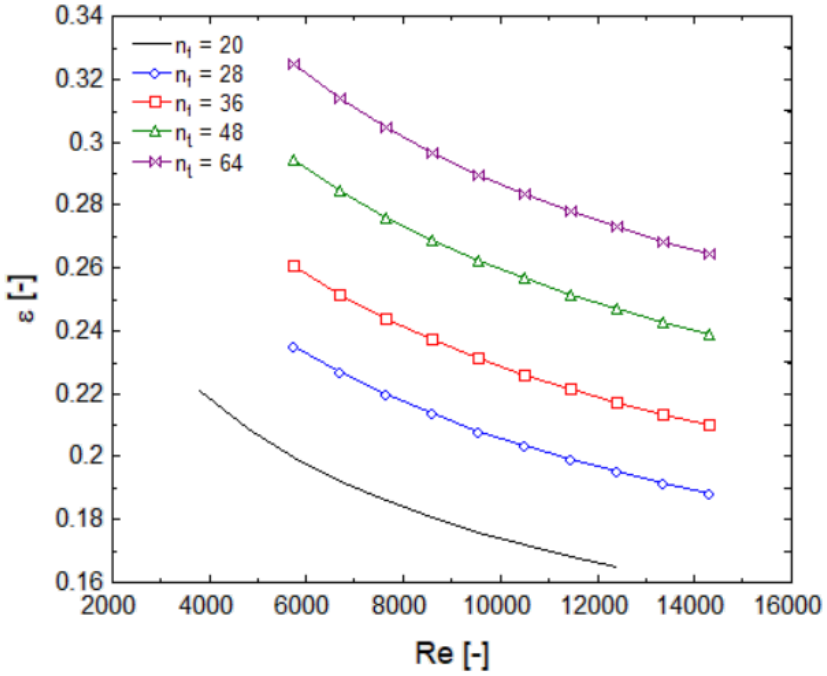

Source: from author.

Figure 8: Profiles for overall thermal conductance *UA* against inlet Reynolds number *Re* obtained for the 5 recuperator geometries.

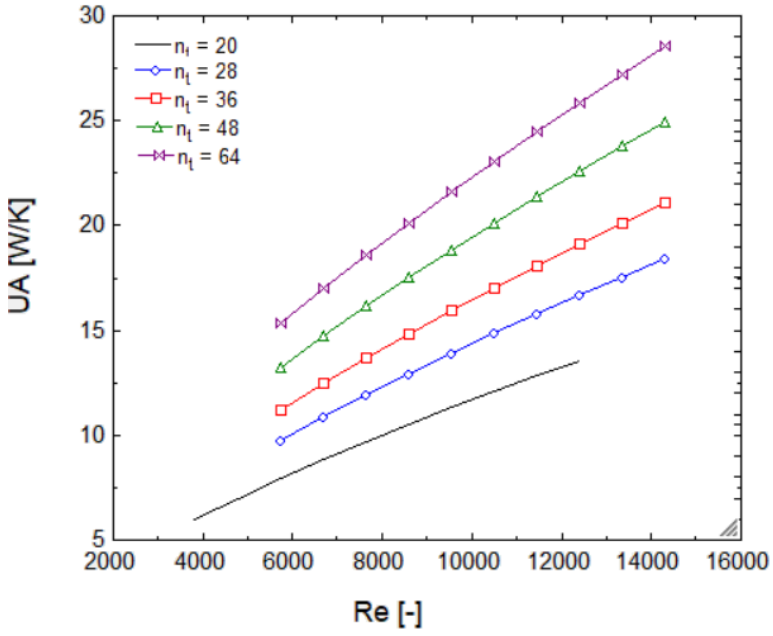

Source: from author.

The convection heat transfer coefficient h and the Colburn factor j characterize heat transfer within a solid-fluid interface, thus it is studied individually for the surface between the HX cold side in the tubes inner walls and for the surface between the tubes outer walls and the HX hot side. Figure 9 displays the results for the cold side convection coefficient h_c distributed by HX geometry against inlet Reynolds number *Re*. This parameter rises with mass flow rate for all geometries, which is expected since advection is enhanced by fluid velocity increase, which also collaborates for the increment of the overall thermal conductance. The increase in number of tubes has a negative impact on h_c because the tube flow is distributed in a greater cross-sectional area in geometries with a higher n_t, which, for the conditions under study (fixed inlet mass flow rate), causes flow velocity fall and yields a lower h_c. Nevertheless, the Q e UA results reveal that the convection coefficient loss is compensated by the heat transfer area enhancement.

Figure 10 shows the results for the hot side convection coefficient h_h. Similarly to the cold side case, the convection coefficient on the hot side increases with flow velocity and falls with the number of tubes. The latter is explained by the increase in the number of stagnation regions next to the tubes outer walls as the quantity of tubes increases, which is responsible for decreasing the mean velocity next to the hot fluid-tube wall surfaces. It can be seen that h_c and h_h are closer in the geometries with more tubes, which indicates that the exchanger convection heat transfer phenomena is more well-balanced in these geometries.

Figure 9: Profiles for cold stream convection heat transfer coefficient h_c against inlet Reynolds number *Re* obtained for the 5 recuperator geometries.

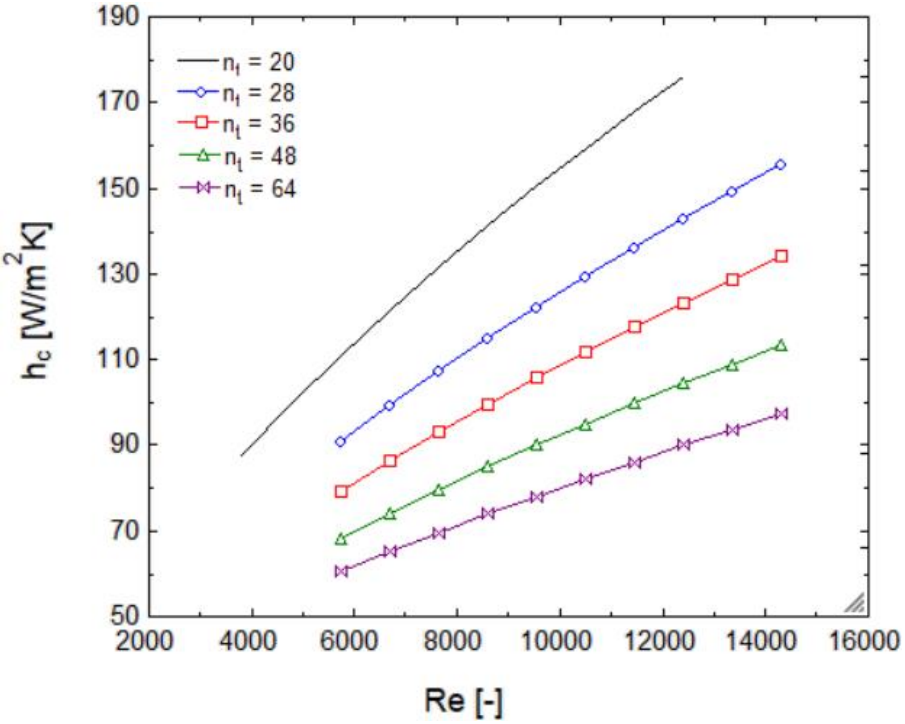

Source: from author.

Figure 10: Profiles for hot stream convection heat transfer coefficient h_h against inlet Reynolds number *Re* obtained for the 5 recuperator geometries.

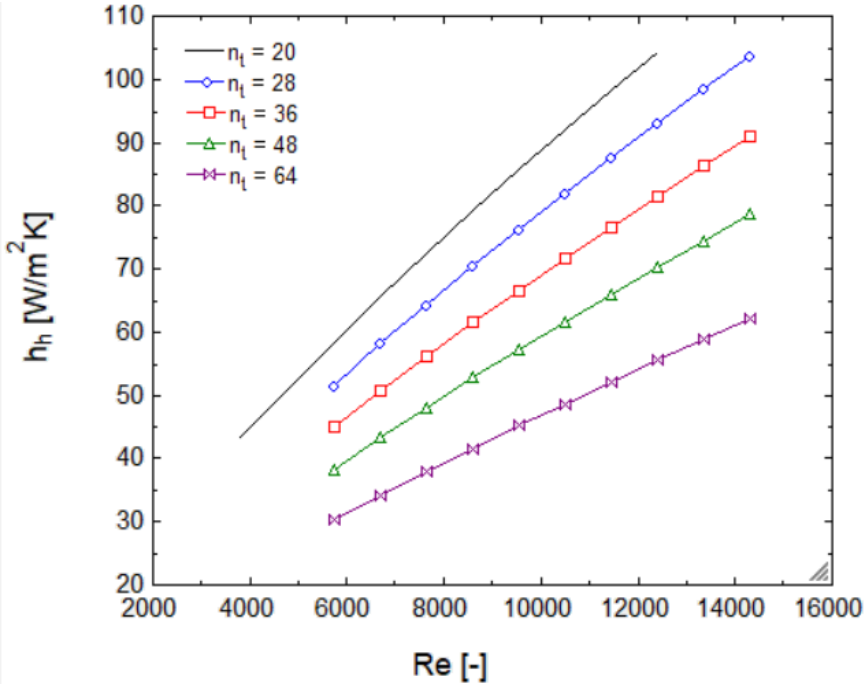

Source: from author.

Figure 11 describes the cold side Colburn factor j_c results in function of inlet Reynolds number *Re*. The j_c values decrease with flow velocity for all the tested geometries, mainly in lower mass flow rate regimes, which indicates a decrease in the ratio between the convected heat transfer to the cold fluid and the demanded fluid bulk enthalpy change for wall temperature reach. This was expected as the effectiveness is shown to decrease with mass flow rate like described graphically in fig. 7.

The hot side Colburn factor j_h curves are displayed in fig. 12. Oppositely to the cold side results, the value of j_h decreases with number of tubes, which occurs because of the HX shell geometry, where the majority of the hot side domain is far from the tube walls. In this scenario, the temperature of the tubes outer walls falls more intensely than the bulk shell side flow temperature as n_t increases.

Figure 11: Profiles for cold stream Colburn factor j_c against inlet Reynolds number *Re* obtained for the 5 recuperator geometries.

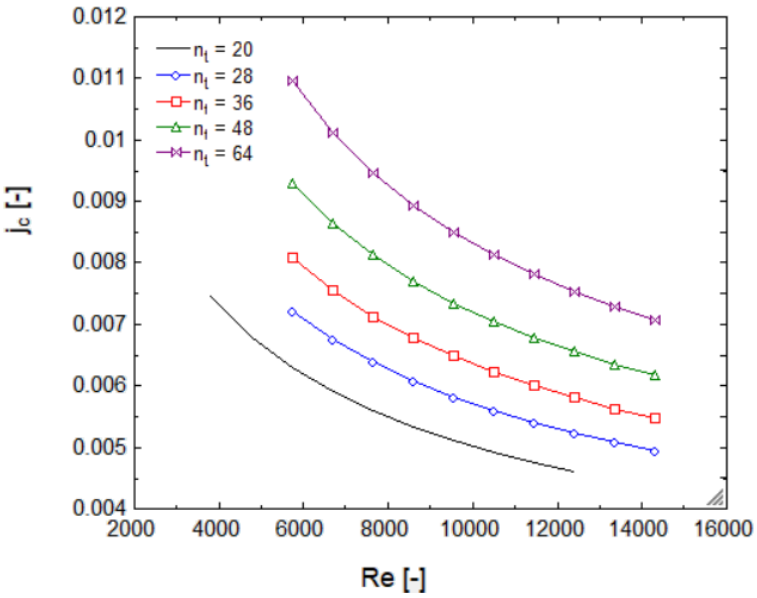

Source: from author.

Figure 12: Profiles for hot stream Colburn factor j_h against inlet Reynolds number *Re* obtained for the 5 recuperator geometries.

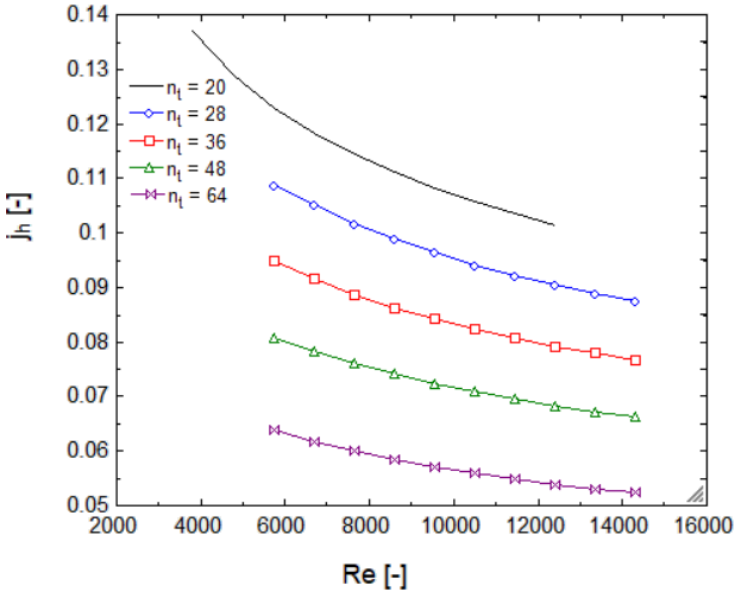

Source: from author.

4. CONCLUSIONS

This work describes the assessment of the thermal performance associated with of a cross flow heat exchanger used as the recuperator of a Closed Brayton Cycle applicable for space nuclear reactors. It draws motivation from the growing interest towards the development of efficient thermal cycles to attend compact nuclear reactors applicable for space.

This study is initially consisted by the construction of a CFD model using data from prior documentation on space nuclear designs applying a similar technology, followed by the creation of a mesh that could satisfy quality criteria and represent the heat transfer and flow phenomena with acceptable fidelity. This grid is validated through a mesh independence check. The flow is solved through the Finite Volume Method under a commercial CFD platform (Ansys Fluent) and the obtained results on the HX temperature field are used as inputs to equations from heat transfer theory in order to characterize the exchanger heat transfer by its main thermal parameters: heat transfer rate Q, effectiveness ε, overall thermal conductance UA, convection heat transfer coefficient h and Colburn factor j. The main conclusions obtained in this work are:

- Heat transfer rate raises with number of tubes in a regular fashion due to superficial area increment and rises with flow velocity due to the increase in the fluid flow rate under a fixed inlet temperature difference.
- Effectiveness values falls with flow velocity because due to the increase of heat capacity rate. It rises with number of tubes because of the heat transfer area augmentation.
- The effectiveness results (~ 0.4) are considerably lower than the ones associated to heat exchangers used in CBCs applicable for space nuclear reactors found in the literature (~ 0.9), which suggests a need for a HX geometry re-design, with the inclusion of heat transfer enhancement features, such as fins, for example.
- The Overall Thermal Conductance follows a similar pattern to that of Q regarding both number of tubes and flow velocity.
- The cold side convection coefficient falls with number of tubes in a decreasing rate and rises with flow velocity, which occurs because a n_t increase reduces the bulk flow velocity inside the tubes. The hot side convection coefficient falls with n_t due to the creation of stagnation region close to the tube walls, which reduces flow velocity in

these regions. The convection heat transfer is approximately balanced in geometries with higher n_t because of the closeness between h_c and h_h values.

- The cold side Colburn factor increases with number of tubes and falls with mass flow rate, which occurs because heat transfer area increase is responsible for rising the fluid temperature range, but flow velocity increase lowers the HX effectiveness and the consequently the fluid enthalpy rise relatively to the wall temperature. The hot side Colburn factor falls with number of tubes and inlet Reynolds number. The former is explained by the HX shell geometry, where the majority of the domain is far from the tube walls, thus heat transfer augmentation through n_t rise causes tubes external walls mean temperature to decrease in a higher rate than the hot stream temperature.

The following works are suggested for researchers who might be interested in developing new findings after the results of this work:

- Validate experimentally the temperature field obtained numerically;
- Perform parametrical studies for a range of inlet temperatures;
- Evaluate thermal performance with other working fluids;
- Perform transient simulations with the used CFD model;
- Design and test geometries with finned tubes for effectiveness and overall thermal conductance increase;
- Compare the results of this work with the ones obtained from simulations performed in open-source CFD codes as OpenFOAM and SU2.

ACKNOWLEDGMENT

This research is part of the TERRA project (from Portuguese, an acronym for Advanced Fast Reactor Technology), supported by the Brazilian Air Force – FAB, which is acknowledged in this work. The authors would also like to thank the financial support of the National Council for Scientific and Technological Development – CNPq.

REFERENCES

[1] MCCLURE, P. R.; POSTON D. Design and testing of small nuclear reactors for defense applications, In: **INVITED TALK TO ANS TRINITY SECTION**, 2011, American Nuclear Society.

[2] ARAÚJO, E. F.; GUIMARÃES, L.N.F. American space nuclear electric systems. **Journal of Aerospace Technology and Management**, 10:e4418, 2018.

[3] FAN, S.; LI, M.; ZHOU, T.; WU, Y.; WU, S. Thermodynamic analysis and optimization of a Stirling cycle for lunar surface nuclear power system. **Applied Thermal Engineering**, v. 111, p. 60-67, 2017.

[4] TORO, C; LIOR, N. Analysis and comparison of a solar-heat driven Stirling, Brayton and Rankine cycles for space power generation. **Energy**, v. 120, p. 549-564, 2017.

[5] TARLECKI, J.; LIOR, N.; ZHANG, N. Analysis of thermal cycles and working fluids for power generation in space. **Energy Conversion and Management**, v. 48, p. 2864-2878, 2007.

[6] GALLO, B. M.; EL-GENK, M. S. Brayton rotating units for space reactor power systems. **Energy Conversion and Management**, v. 50, p. 2210-2232, 2009.

[7] AHN, Y.; LEE, J. I. Study of various Brayton cycle designs for small modular sodium-cooled fast reactor, **Nuclear Engineering and Design**, v. 276, p. 128-141, 2014.

[8] GOODARZI, M. Usefullness analysis on recuperator and heat exchanger in Brayton & inverse Brayton cycles at moderate pressure ratio operation. **Nuclear Engineering and Design**, v. 276, p. 128-141, v. 2014.

[9] OLUMAYEGUN, O.; WANG, M.; KELSALL, G. Thermodynamic analysis and preliminary design of a closed Brayton using nitrogen as working fluid and coupled to small modular sodium-cooled fast reactor (SM-SFR). **Applied Energy**, v. 191, p. 436-453, 2017.

[10] DIXIT, T.; GHOGH, I. Review of micro- and mini-channel heat sinks and heat exchangers for single pass phase fluids. **Renewable & Sustainable Energy Reviews,** v. 41, p. 1298-403, 2016.

[11] OZDEN, E.; TARI, I. Shell side CFD analysis of a small shell-and-tube heat exchanger. **Energy Conversion and Management**, v. 51, pp. 1004-1014, 2010.

[12] LIU, C.; BU, W.; XU, D. Multi-objective shape optimization of plate-fin heat exchanger using CFD and multi-objective algorithm. **International Journal of Heat and Mass Transfer**, v. 111, p. 65-82, 2017.

[13] ZHANG, X.; SAEED, M.; YU, J. A CFD-based simulation of fluid flow and heat transfer in the intermediate heat exchanger of sodium-cooled fast reactor, **Annals of Nuclear Energy**, v. 109, p. 529-537, 2017.

[14] MORTEAN, M. V. V.; CISTERNA, L. H. R.; PAIVA, K. V.; MANTELLI, M. B. H. Thermal and hydrodynamic analysis of a cross-flow compact heat exchanger. **Applied Thermal Engineering**, v. 150, p. 750-761, 2019.

[15] PATANKAR, S. V. **Numerical Heat Transfer and Fluid Flow**, 1st ed. New York: MCGraw-Hill, 1980.

[16] VERSTEEG, H. K.; MALALASEKERA. **An Introduction to Computational Fluid Dynamics**, 2nd ed. Harlow: Pearson Prentice Hall, 2017.

[17] GUIMARÃES, L. N. F.; CAMILLO, G. P.; PLACCO, G. M. Design of a Simplified Closed Brayton Cycle for a Space Reactor Application, In: **SPACE, PROPULSION AND ENERGY SCIENCES INTERNATIONAL FORUM**, 2009, Huntsville. Proceedings…Huntsville: University of New Mexico Institute for Space and Nuclear Power Studies.

[18] ASHE, T. L.; BAGGENSTOSS, W. G.; BONS, R. Nuclear Reactor Closed Brayton Cycle Power Conversion System Optimization Trends for Extra-Terrestrial Applications, In: **25th ENERGY CONVERSION ENGINEERING CONFERENCE**, 1990, Reno. Proceedings…Reno: American Institute of Chemical Engineers.

[19] ASHCROFT, J. ; ESHELMAN, C. Summary of NR Program Prometheus Efforts. In: **SPACE, PROPULSION AND ENERGY SCIENCES INTERNATIONAL FORUM**, 2007, Huntsville. Proceedings…Huntsville: University of New Mexico Institute for Space and Nuclear Power Studies.

[20] WRIGHT J. K.; LILLO, T. M. Creep and Creep-rupture of Alloy-617. **Nuclear Engineering and Design**, v. 329, p. 142-146, 2018.

[21] EL-GENK, M. S.; TOURNIER, J. M. Noble gas binary mixtures for gas-cooled reactor power plants. **Nuclear Engineering and Design**, v. 238, p. 833-849, 2007.

[22] High Temp Metals Inc. **Inconel 617 technical data**. Sylmar, California, USA. 2015. Available at: < http://www.hightempmetals.com/techdata/hitempInconel617data.php>. Last accessed : 27 May 2020.

[23] SHAH, R. K.; SEKULIC, D. P. **Fundamentals of heat exchanger design**, 1st ed. New York: John Wyley & Sons, 2003.

[24] INCROPERA, F. P.; DEWITT, D. P.; BERGMAN, T. L.; LAVINE, A. S. **Fundamentals of heat and mass transfer**, 7th ed. New York: John Wyley & Sons, 2007.